20

Photodetectors in Calorimeters for the Linear Collider

Jaroslav Cvach and CALICE Collaboration
Institute of Physics of the ASCR, v.v.i., Praha
Czech Republic

1. Introduction

The next high energy accelerator that will be built after the Large Hadron Collider currently operating at CERN is expected to be a Linear Collider (LC). It is envisaged to be an electron-positron colliding beams facility with the centre-of-mass energy of 500–3000 GeV (ILC, 2007, Vol. 3; CLIC, 2011). The detector at the LC will have to deal with a large dynamic range in particle energy, complexity of final states and small signal-to-background ratio. The track density in collimated jets can be as high as one per mm^2 at a radius of 1.5 cm, and the accelerator induced backgrounds produce typical hit densities of the order of 0.03/mm^2 per bunch crossing at a radius of 1.5 cm, and 0.003/cm^2 at a radius of 30 cm. The physics requirements demand detector performance parameters which must be substantially better than at previous experiments on accelerators at the large electron-positron collider in CERN and at the Stanford linear collider in SLAC. The goal is to achieve the energy resolution for jets $\sigma/E < 3\%$ in wide range of energies starting from the mass of the intermediate bosons W and Z, $E \sim m_W$, $m_Z \sim 80$ GeV to several hundred GeV. This condition is often translated into the formula used for the energy resolution of the sandwich calorimeter $\sigma/E \sim 30\%/\sqrt{E}$ (jet energy E is in GeV).

The experimental technique proposed to reach these goals was formulated ten years ago and is now known as the particle flow algorithm (PFA) (Brient & Videau, 2001; Cvach, 2002; Morgunov, 2002). The PFA combines the information from tracking and calorimetry to obtain an optimal estimate of the flow of particles from the interaction vertex and of the original parton four-momenta. The subdetectors must have excellent spatial granularity to enable a PFA algorithm which resolves energy depositions of almost overlapping particles, combines redundant measurements properly (e.g. of electrons in tracking and the electromagnetic calorimeter or of charged pions in tracking and calorimetry) and provides other corrections (e.g. calorimeter software compensation). The calorimeter for experiments at the LC must be realized as a dense and hermetic sampling calorimeter with a very high granularity, where one can efficiently separate the contributions of different particles in a jet and use the best suited detector to measure their four-momenta.

In this article we review the performance of modern photodetectors used in already built calorimeter prototypes with plastic scintillator as the active medium. Calorimeters are constructed as a sandwich with an absorber between the scintillator layers to decrease the calorimeter size.

2. Calorimeter prototypes optimized for the PFA

The CALICE collaboration (Calice, n.d.) has undertaken an intensive R&D program starting in 2001 to prove feasibility of the particle flow approach for the improvement of detector energy resolution by a factor of approximately two for jets produced in e^+e^- collisions at centre of mass energies 50-1000 GeV. The corresponding effort was done both on the subdetector side as well as on the software side – reconstruction and simulation programs. We shall concentrate in this article on calorimeters optimized for the PFA. For effective functioning of a calorimeter, the vertex tracker and tracker standing in front of calorimeters are important. We refer e.g. to (ILC, 2007, Vol. 4) where relevant solutions for trackers are discussed in detail.

The first completed prototype of the electromagnetic calorimeter ECAL was SiW ECAL (Repond et. al., 2008). The large silicon diode sensors of 1x1 cm^2 area made on high resistive Si wafers 0.5 mm thick define the size of the active calorimeter cell. A sensitive area of 18x18 cm^2 of silicon was inserted between absorber tungsten plates 1.2-4.8 mm thick. In total 30 layers of Si + W represent 24 radiation lengths X_0. The total number of cells was 9720. As this calorimeter does not use photodetectors, we refer for further details to the latest publication (Adloff et al., 2010b).

As an alternative to the SiW ECAL, a scintillator ECAL was built which used scintillator strips read by Multi-Pixel Photon Counter (MPPC) photodetectors. The absorber is also tungsten and the sensitive area was 18x18 cm^2. The scintillator strips are 1 cm wide and oriented alternatively in x and y directions to make effectively 1 cm^2 cells comparable to SiW ECAL. Thus good comparison between two ECAL realisations can be done. We refer in detail about the scintillator ECAL in section 4.

The first completed prototype of the hadron calorimeter was a 1-m^3 steel-scintillator calorimeter with SiPMs as photodetectors that provide analog amplitude. The optimisation studies for the PFA defined (Thomson, 2009) as the best tile size 3x3 cm^2. For the economical and practical reasons, the prototype was built from tiles of three different sizes made of 5 mm thick scintillator placed between steel absorber plates 16 mm thick. 38 sandwich layers have a depth of 1 m and represent 5.3 interaction lengths. The details are given in section 5.

Recently two versions of calorimeter with the scintillator replaced by the gas detector – Resistive Plate Chamber (RPC) – were completed and are currently tested in beam. As the RPC provides digital amplitude from a 1 cm^2 cell, we call this type of calorimeter digital. Further details are given in references (Bilki et al., 2009; Laktineh, 2011).

3. Silicon photomultiplier

The CALICE collaboration contributed to the first massive use of a novel multi-pixel silicon photodetector operated in the Geiger mode. There are several producers able to deliver this photodetector, e.g. Hamamatsu Photonics Japan (first commercial producer), MEPHI/PULSAR and Dubna/Micron in Russia, Photonique in Switzerland, SENSL in Ireland, ITC IRST Trento in Italy, Zecotek in Singapur, MPI Semiconductor Laboratory Munich in Germany, SensL Cork in Ireland, STmicroelectronics in Italy, Novel Device Laboratory Beijing in China, RMD Boston in U.S.A., and possibly others.

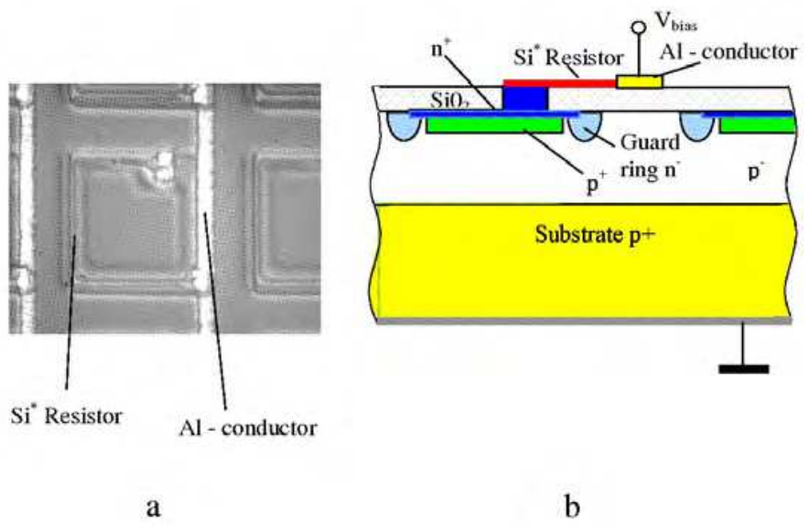

Fig. 1. (a) View of a pixel in an array of the silicon photomultiplier. (b) A cross section of a pixel of SiPM showing the layers. The Si* resistor serves as a quenching resistor, the SiO2 resistor reduces the inter pixel cross talk.

We shall here report about experimentation with the Silicon PhotoMultiplier (SiPM) from MEPHI/PULSAR which delivered more than 10000 pieces for the Analog Hadron CALorimeter (AHCAL) and the Tail Catcher and Muon Tracker (TCMT) and the Pixelated Photon Counter from Hamamatsu whose 2160 pieces of the "1600-pixel MPPC" were used in the Scintillator Electromagnetic CALorimeter (ScECAL).

The silicon photomultiplier is an array of small pixels connected on a common substrate (see Fig. 1). Each cell has its quenching resistor of the order of a MΩ. A common bias voltage is applied to all cells 10-20% above the breaking voltage. The cells fire independently when a carrier is liberated in the depletion layer or by a photon arriving on the surface or thermally. The output signal equals to the sum of fired cells. At small signals the detector works as an analog photodetector, at large signals the detector saturates due to the limited number of pixels (Bondarenko et al., 2000; Buzhan et al., 2001) The photon detection efficiency is $\varepsilon = QE\ \varepsilon_{geom}$, where quantum efficiency QE is 0.5-0.8 and ε_{geom} is geometrical factor giving the effective sensitive area of the pixel. The geometrical factor increased from originally several percents up to 80% nowadays (Musienko, 2011). Each pixel works as a digital device – several photons hitting the same pixel produce the same signal as a single photon. Optical cross-talk between pixels causes adjacent pixels to be fired. This increases gain fluctuation, increases noise and excess noise factors. Due to the Geiger discharge, the pulse is short, typically several ns long. The photodetector for the AHCAL prototype was developed in collaboration of Moscow Institutes MEPhI and ITEP with PULSAR factory near Moscow and with support from DESY Hamburg. They called it silicon photomultiplier because of its high gain. The photosensitive area of 1.1 mm x 1.1 mm holds 1156 pixels each having an area 32 μm x 32 μm (sensitive area 24 μm x 24 μm). The single pixel signal is determined by the total charge collected during the Geiger discharge $Q = C_{pixel}\,\Delta V$ where ΔV is the voltage above the breakdown voltage V_{break}. For the pixel capacitance C_{pixel} = 50 fF and ΔV = 3V the signal reaches Q = 150 fC ~ 10^6 electrons. This defines the gain of ~ 10^6. The working voltage equals to $V_{bias} = V_{break} + \Delta V$ ~ 50-60 V. The cross talk increases with ΔV, the typical value is

20%. The Geiger discharge time is ~ 500 ps. The pixel recovery time is defined by the product C_{pixel} R_{pixel} , where R_{pixel} is the pixel quenching resistor (400 kΩ - 10 MΩ). The quenching resistor interrupts the discharge in a pixel. For smaller resistor values the quenching time is ~ 20 ns.

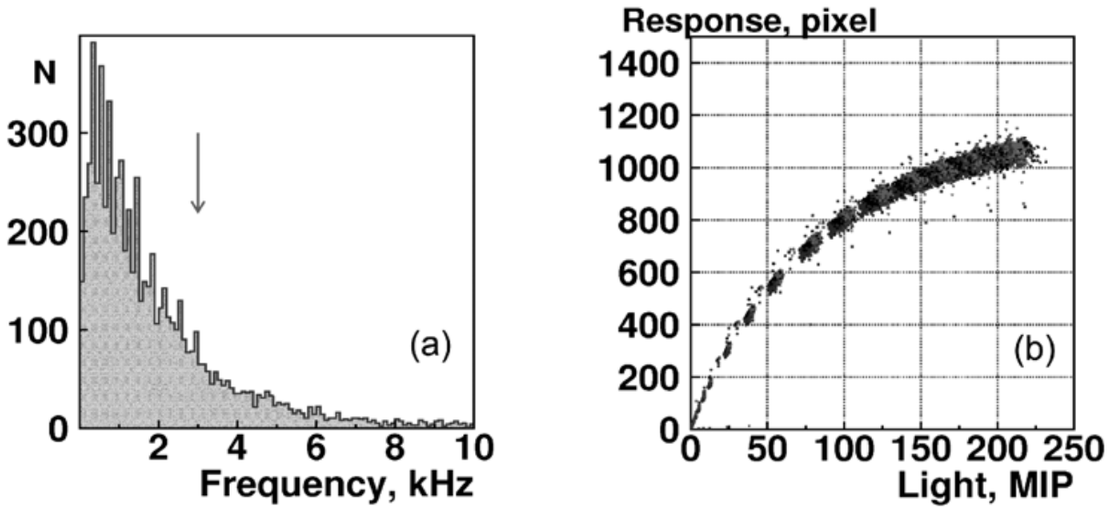

Fig. 2. (a) Distribution of noise above ½ MIP threshold for 10000 SiPMs produced in MEPHi/PULSAR. The arrow at 3 kHz shows selection cut. SiPMs with higher noise were discarded. (b) The response curve for the selected SiPMs. The curve shows the SiPM signal in number of fired pixels as a function of the LED light expressed in MIPs.

The aim was to keep it below 100 ns with the signal width of ~ 10 ns. For short recovery times comparable to the signal width, the SiPM can fire repeatedly causing undesirable inter pixel crosstalk. The pixels are connected in parallel to one readout channel therefore the output pulse is proportional to the number of detected photons (Danilov, 2007b).

More than 10000 SiPM have been produced by the MEPhI/PULSAR group and were tested at ITEP. The SiPMs were illuminated with calibrated light from a UV LED (Ultra-Violet Light Emitting Diode). The light was brought by a Kuraray Y11 WLS fibre. For each SiPM the working voltage was chosen individually to fire 15 pixels for LED light pulse corresponding to the signal which produces a minimum ionizing particle (MIP) - in practice a muon - in a scintillator tile. The gain, the dark rate, the inter-pixel crosstalk, the noise above a threshold of the ½ MIP and the non-linear response function were measured for all SiPMs. The SiPMs had to fulfil selection criteria on gain > 4.10^5, noise at ½ MIP threshold < 3 kHz, cross talk probability < 0.35 and dark current < 2.10^{-6} A. As an example in Fig. 2a the noise distribution is shown, the arrow gives the position for the selection cut.

SiPMs were tested for radiation hardness on the proton accelerator at ITEP Moscow at a beam energy of 200 MeV. The dark current of SiPMs increased with the proton flux Φ as expected. At doses $\Phi \sim 10^{10}$ protons/cm^2 the detector does not see individual photoelectron peaks and still resolves MIPs at $\Phi \sim 10^{11}$ protons/cm^2. This radiation hardness is sufficient for doses the AHCAL will obtain at the LC (Danilov, 2007a).

Photodetectors for the ScECAL were developed by cooperation between the Shinshu University and the Hamamatsu Photonics Company. The MPPC has a photon detection area

of 1 mm x 1 mm with 1600 pixels. The delivery was realised in two batches. The smaller batch in 2006 comprised 532 pieces for test purposes of a small calorimeter in the DESY test beam. The main delivery of ~ 2000 pieces was carried out in 2008. Some of the MPPCs from the DESY test set up (448 pieces) were used also in the ScECAL. The characteristics of MPPCs were measured in the pulse mode in a test stand using LED flashes controlled by a pulser. The MPPC temperature was kept at 25°C in a thermostat. The distribution of gain and crosstalk for three MPPC groups is shown in Fig. 3 (Sakuma, 2010). The MPPC properties depend on the production batch but within the same batch they exhibit low spread. The different MPPC gain between two production batches was equalized in the calorimeter by adjusting the individual bias voltage setting for each MPPC. This is done by the front-end ASIC chip.

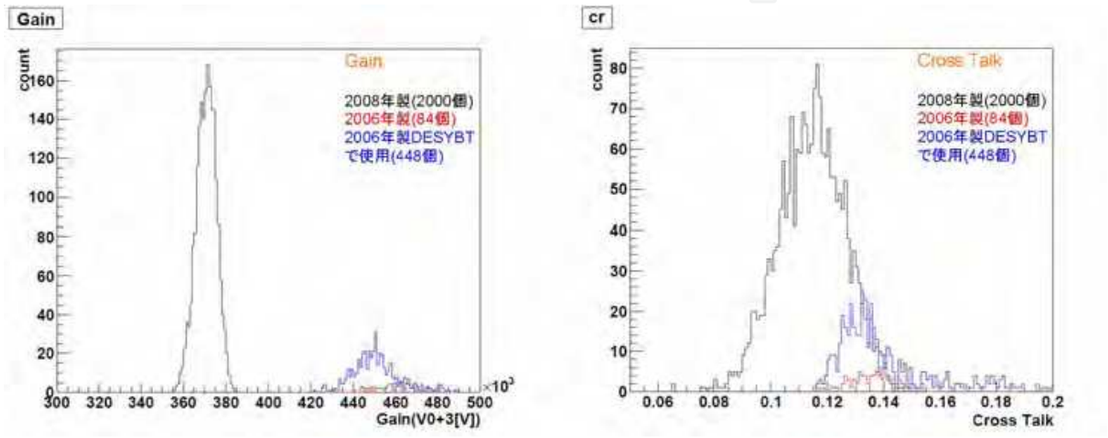

Fig. 3. Distribution of gain (left) and cross-talk (right) for MPPCs produced in Hamamatsu and used in the ScECAL. The production was done in years 2006 and 2008. 448 MPPCs from 2006 and all from 2008 were used in the ScECAL.

The SiPM becomes saturated at large photoelectron intensities N_{ph} due to the limited number of pixels N_{avail}. From the probability considerations the number of fired pixels N_{pix} increases exponentially with N_{ph} as $N_{pix} = N_{avail} (1 - \exp(-N_{ph} / N_{avail}))$. The measured dependence of the response curve N_{pix} (N_{ph}) for 10000 SiPMs is given in Fig. 2b. The inverse of this dependence is used as a correction function of the measured signal N_{pix} to get the effective number of photoelectrons N_{ph}. For more sophisticated treatment of the saturation correction see section 8.

4. Scintillator electromagnetic calorimeter

The most important role of the Electromagnetic Calorimeter (ECAL) is to identify photons in jets. The majority of photons are produced by two-photon decay of the neutral pions. The distance between two photons decreases with increasing pion energy and it is several centimetres at the distance 210 cm from the decay point for pion energy several tens of GeV. Therefore, the ECAL granularity around 1 cm will allow resolution of photons from pions up to energies of about 50 GeV.

The ScECAL was built with 1 cm x 4.5 cm scintillator strips 0.3 cm thick assembled from 18 pieces in 4 rows into a plane. Each strip is wrapped in reflecting foil to isolate it from the

neighbour and to improve the light collection. Scintillation light is read by a wavelength shifting (WLS) fibre placed in the middle of the strip along its longer side to improve the homogeneity of the light collection. The calorimeter is made of 30 layers with strips alternately rotated by 90 degrees. In between two scintillator planes, tungsten absorber plane 0.35 cm thick, is inserted (see Fig. 4).

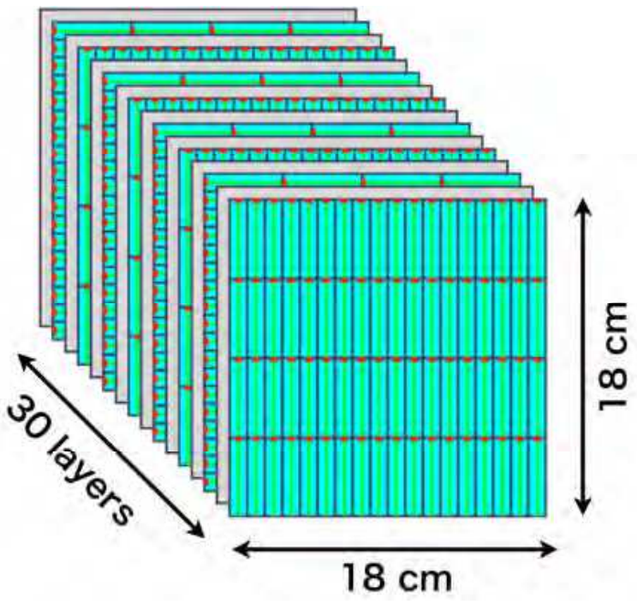

Fig. 4. Scintillator ECAL structure. The scintillator strips (green) are arranged in 4 rows by 18 pieces to form a plane. WLS fibers in yellow lead light to MPPC (red spot) at the strip end. The W absorber planes are shown in grey.

The WLS double clad fibre contains Y11 wavelength shifter and emits light at 550 nm. The fibre is read at one end by a MPPC. The MPPC has a photon detection area of 1 mm x 1 mm with 1600 pixels. The MPPCs were soldered on a flat cable and mounted at the end of each fibre. Test were also made where the MPPCs were attached directly to the tile as the loss in the light collection from the missing WLS can be partly regained by a better match in peak sensitivity of MPPC (at 400 nm) to the scintillation light. The number of photoelectrons dropped to one half but a significant simplification in construction can be achieved.

The readout of the calorimeter uses the same electronics as the AHCAL and it is described in the next section. The basic eighteen channel front-end ASIC chip reads out in this case one row of scintillators. The prototype of the ScECAL had 2160 MPPCs and it was built in collaboration of Shinshu, Kobe, Tsukuba, Tokyo, Niagata Universities in Japan and Kyungpook National University in Korea (Kotera, 2010).

The calorimeter has been tested in muon and electron beams at energies 1–32 GeV, pion beam 2-60 GeV energy (including neutral pions) in Fermilab in 2008–9. The detector was calibrated using muons to measure the energy response of a MIP. The light yield of 23 photoelectrons was measured for a minimum ionizing particle. The data were further corrected for the saturation (see section 8). The response of the whole calorimeter to several electron beam energies is shown in Fig. 5. The data show clear Gaussian behaviour for individual energy.

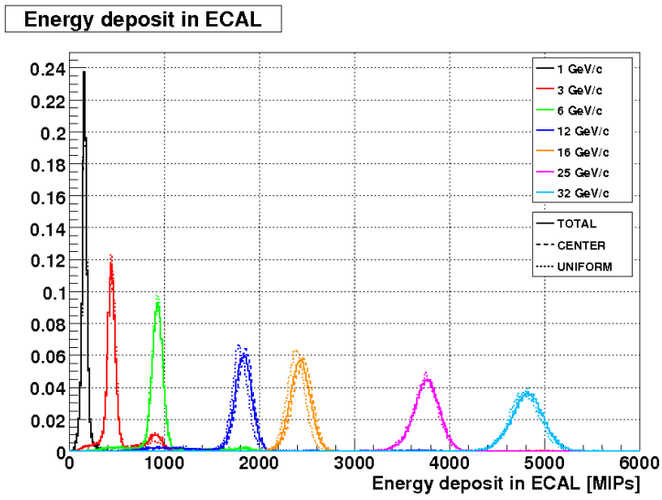

Fig. 5. The corrected energy spectra measured with ScECAL at energies 1–32 GeV.

The data were then purified for small contamination from other particles in the beam namely muons and electrons. The energy distribution was fitted for each energy with a Gaussian function including 90% of data around the Gaussian maximum to further suppress residual contamination (lowest energy point at 1 GeV required a more refined procedure). The deposited energy in the calorimeter is given as the mean of Gaussian function from the fit and the resolution by the standard deviation σ.

The mean of the Gaussian for each beam momentum is displayed in Fig. 6 (left). The points were fitted by a linear function forced to go through the origin. The points differ from the fit at most by 6% at the highest energies. The sources of the nonlinearity are temperature dependence of sensors, spread in saturation correction of sensors and spread in calibration

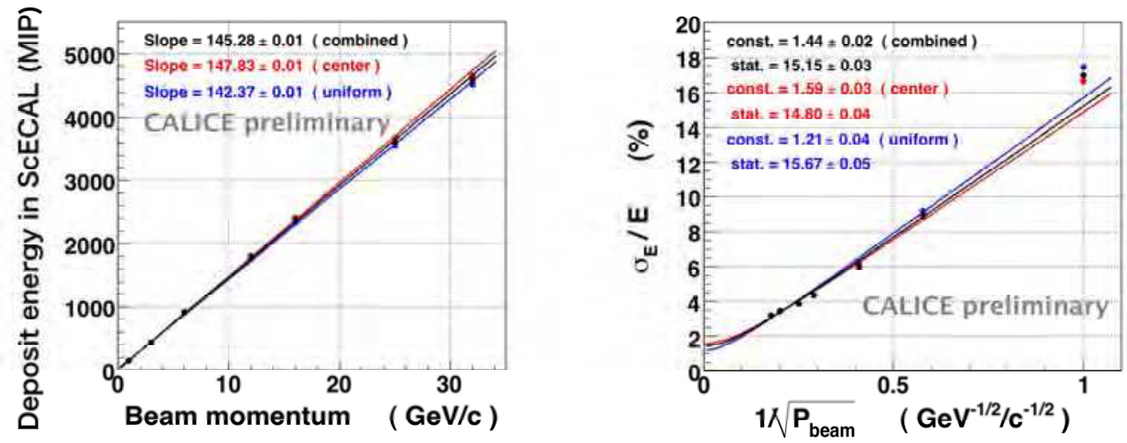

Fig. 6. (left) Linearity response of the ScECAL. Blue (red) data correspond to the beam shot uniformly on (at the center of) the front face of the calorimeter, black are data combined together. (right) The energy resolution of ScECAL as a function of the inverse of the square root of the beam momentum. The formula fitted to data points is quadratic and it is explained in the text.

factors for strips. The sources of the nonlinearity are being further investigated. The calorimeter energy resolution σ_E/E is plotted in Fig. 6 (right) as a function of $\sqrt{(1/P_{\text{beam}})}$. Data at different beam momenta were fitted to the quadratic formula $\sigma_E/E = \sigma_{\text{const}} \oplus \sigma_{\text{stat}}/\sqrt{(P_{\text{beam}})}$, where σ_{const} (σ_{stat}) represent constant and stochastic term in the calorimeter energy resolution and $A \oplus B = \sqrt{(A^2+B^2)}$. Non-zero σ_{const} describes the effect of non-uniformities in the calorimeter (mechanical or due to physics, i.e. different response to electrons and hadrons). The value of σ_{stat} depends on the ratio of scintillator and absorber thicknesses and it is called the 'stochastic coefficient'. It is due to the sampling fluctuations of particle showers in the active medium. The values obtained from tests are σ_{const} = (1.44±0.02)% and σ_{stat} = (15.15±0.03)%. The value σ_{const} is slightly worse than the value 1.07% obtained for a similar calorimeter using 1 cm x 1 cm Si diodes (Repond et al., 2008). The value σ_{stat} is better than the value 16.53% from the SiW calorimeter. The fact that the ScECAL uses 4 times fewer channels which are cheaper to produce and shows a similar performance makes this type of calorimeter a very attractive candidate for the electromagnetic calorimeter in the detector at the LC.

5. Analog hadron calorimeter

The most important task of the hadron calorimeter is to separate the contributions from deposits of charged and neutral hadrons in the hadron shower and to measure the energy of neutral particles. The choice of parts for the physics prototype was a compromise between performance, price and availability. The scintillator chosen comes from UNIPLAST Russia (polystyrene + 1.5% PTO + 0.01% POPOP), the WLS fibre of 1 mm diameter is Kuraray Y11(200) in a groove with ¼ circle for the smallest tiles and with 1 loop for the larger tiles. Before bending the fibre was heated to ~ 80° C.

One layer of the sampling structure of the tile AHCAL physics prototype calorimeter consists of a 16 mm thick absorber plate made from stainless steel and a steel cassette of 96 cm x 96 cm area with two 2 mm thick steel walls to house a plane made from 5 mm thick scintillator tiles. The calorimeter is built as a cube of approximately 1 m^3 volume. The total number of 38 layers corresponds to 5.3 interaction lengths λ_{int}. The view of one plane with scintillator tiles is shown in Fig. 7 left. In the centre where the test beam passes through, one hundred small 3 cm x 3 cm tiles is surrounded by three rows of tiles 6 cm x 6 cm and finally at the perimeter by one row of tiles 12 cm x 12 cm. The tiles at 4 corners were removed as the occupancy is expected to be low. Each tile is coupled via a WLS fibre inserted in a groove to a SiPM via an air gap (Fig. 7 right). The tiles are covered from top and bottom with a super-radiant foil VM2000 from 3M. The tile side edges were matted in order to provide better homogeneity of the light on the photodetector.

One detector plane comprises 216 scintillator tiles closely packed inside a frame made from aluminium bar 10 mm x 8 mm. The SiPMs are connected to the front-end electronics via 50 Ω micro-coax cables that carry both signal and bias voltage. Each tile is also connected to a clear fibre which brings calibration light from LED. Both coax cables and fibres lay on a support FR4 plate covered with a mylar foil for insulation. It means that SiPMs are not soldered on a PCB as this construction is too fragile to carry the mass of the scintillator. The coax cables are connected on one side of the plane to the front-end electronics, eighteen optical fibres are attached on the other side to one LED mounted on the calibration and monitoring board (Adloff et al., 2010a).

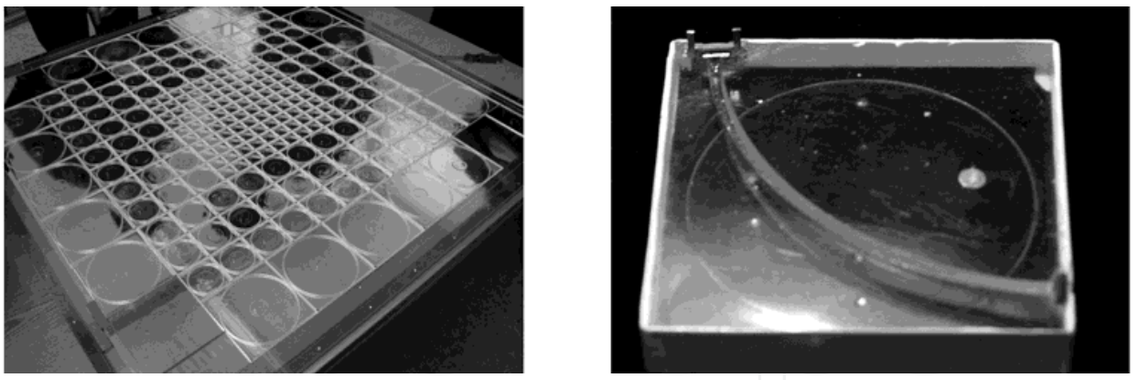

Fig. 7. (left) Scintillator tile layer of the AHCAL calorimeter prototype. The tile of three different sizes can be recognized as well as the WLS fibers of the circular shape inside the tiles. The photodetector SiPM is placed in the tile corner and powered and read-out via connections to micro-coax cable below the scintillators. (right) Scintillator tile 3 cm x 3 cm with a WLS fiber in a groove attached via an air gap to the photodetector SiPM placed in the upper left corner of the tile. Two SiPM contacts are used to bring the bias voltage and the readout of the signal. The other end of the WLS fiber is covered by a reflector to improve the overall light yield.

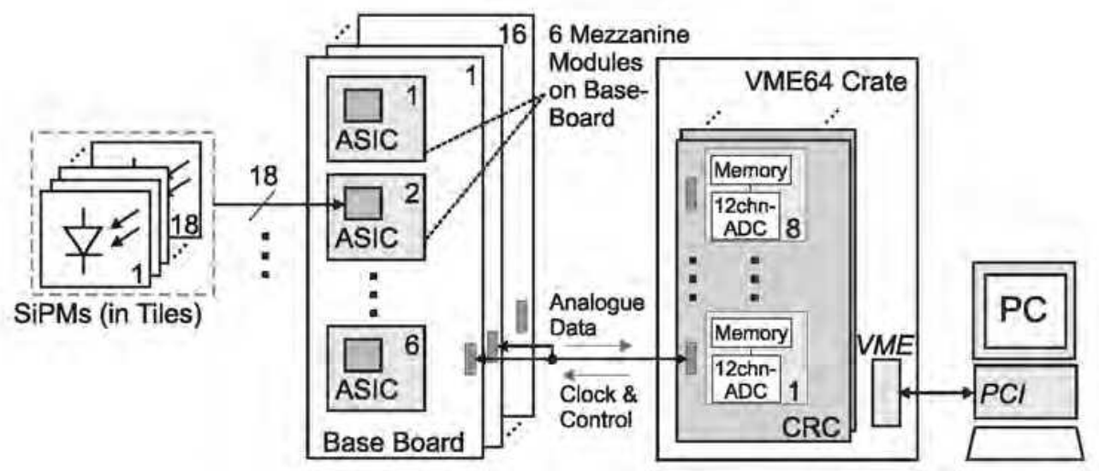

Fig. 8. Schematic view of the readout and data acquisition system of the AHCAL

A schematic view of the readout system is shown in Fig. 8. Eighteen SiPMs are connected to the same ASIC (de La Taille et al., 2005**)** which has for each SiPM preamplifier, shaper and sample-and-hold-circuit. It also allows individual bias voltage settings for each SiPM. It is made in the 0.8 μm Complementary Metal-Oxide-Semiconductor (CMOS) technology. The signals from twelve Application-Specific Integrated Circuits (ASICs) are fed into the CALICE Readout Card (CRC) and digitized by 16-bit Amplitude Digital Converters (ADCs). The data are stored via a PC, which controls also the data taking. The construction of the physics prototype and the readout and data acquisition system is a common effort of DESY, Hamburg University, Imperial College London, ITEP, Lebedev Physics Institute and MEPHI Moscow, LAL Orsay, and Institute of Physics Prague.

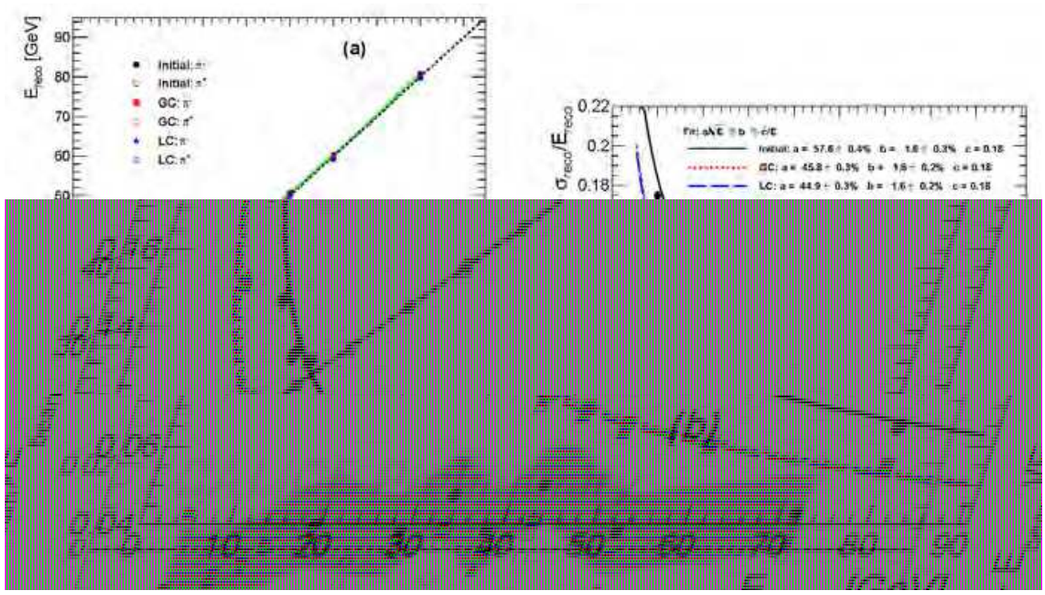

Fig. 9. (left a) Linearity of the AHCAL to pions. (left b) Relative residuals to beam energy versus beam energy. (right) Relative energy resolution of the AHCAL for pions versus beam energy. Black points and lines correspond to analysis without compensation, blue (red) points and curves show results of analysis after local (global) compensation.

The AHCAL was extensively exposed to beams of electrons and hadrons in years 2007-9. All detectors showed high reliability. The calibration and monitoring procedures were validated. At the beginning the calorimeter was calibrated to get the overall energy scale. With help of the wide muon beam each calorimeter cell was exposed to have at least 500 reconstructed muon tracks in the cell. These data were used to obtain the MIP conversion factor expressing the charge measured (in units of ADC counts) by the SiPM in units of MIPs. With low intensity LED light the individual photons (or pixels, see Fig. 10 in section 7) were recorded by the same data acquisition chain and also measured in ADC counts. The operation voltage of SiPMs was set at the value of ~ 13 pixels/MIP to equalize the SiPM response. The factor converting MIP to energy in MeV was obtained from the Monte Carlo simulation and allowed to express the charge measured by SiPM in energy scale in MeV. This energy was finally corrected for the SiPM saturation. The SiPMs proved their reliability and gain stability over the whole period and the whole HCAL showed its robustness during transport between laboratories at DESY, CERN and Fermilab. During the test beam periods at CERN the data were collected in the pion beam in the energy range 8-80 GeV and $e^{\pm}$ beams 6-45 GeV. The pion data were purified, reconstructed and calibrated using the standard CALICE chain (Adloff et al., 2011). To improve the linearity and the energy resolution of the AHCAL, two software correction methods were developed which compensate the AHCAL higher response to electrons $e/\pi = 1.19$. The algorithms use information on the shower substructure and reweight higher local energy deposits by suitable factors on event-by-event basis. The linearity and energy resolution of the complete CALICE setup (ECAL + AHCAL + TCMT) is shown in Fig. 9 for data (black) and data after software compensation correction by the local compensation (blue) and global compensation (red) methods. The response is linear within ± 1.5% with slight improvement due to compensation. The resolution formula fitted to data is $\sigma_E/E = \sigma_{const} \oplus \sigma_{stat}/\sqrt{(E_{beam})} \oplus 0.18/E_{beam}$, E_{beam} in GeV. The last term describes the noise width estimation of the test beam

setup. In this case the effect of compensation is significant. The values of σ_{stat} = 57.6% (44.9%, 45.8%) for the data without (with local, global) the software compensation show that on average the compensation methods improve the energy resolution by 21%. The constant term σ_{const} = 1.6%. (Chadeeva, 2011)

6. Tail catcher and muon tracker

The TCMT is a sandwich calorimeter placed behind the AHCAL. It has also a volume of 1 m^3, but coarser structure than the AHCAL. Steel absorber plates have thickness 2 and 10 cm, the active layer consists of 100 cm long, 5 cm wide extruded scintillator strips 0.5 cm thick. The first 8 sections behind the AHCAL have a similar longitudinal segmentation as the AHCAL and will supplement the AHCAL measurement for the tail-end of the hadron showers. The last 8 coarser sections serve as a prototype of a possible muon detector for any design of the ILC detector. It represents 5.8 interaction lengths.

The scintillation light is read out by parallel WLS fibres of 1.2 mm diameter inserted in the co-extruded holes. The fibre is read at one end by a SiPM of the same type as in the AHCAL. The strips and SiPMs are inserted into cassettes made from 1 mm thick steel, the cassettes are inserted alternately in the x and y directions between absorber plates. The TCMT uses 320 SiPMs in total. Each cassette has inside a LED driver board with 20 UV LEDs, one per strip. The TCMT has been constructed by Fermilab, Northern Illinois University, and DESY (Chakraborty, 2005).

7. Monitoring and calibration

During the data taking with the calorimeter it is important to monitor the stability of the entire read-out system starting from the quality of light transfer between scintillator and photodetector to the read-out electronics. The photodetector gain G significantly changes with temperature as $dG/dT \sim -1.7\%/K$ and with the bias voltage as $dG/dU \sim 2.5\%/0.1V$ (Eigen, 2006), therefore the temperature of the photodetector must be periodically recorded.

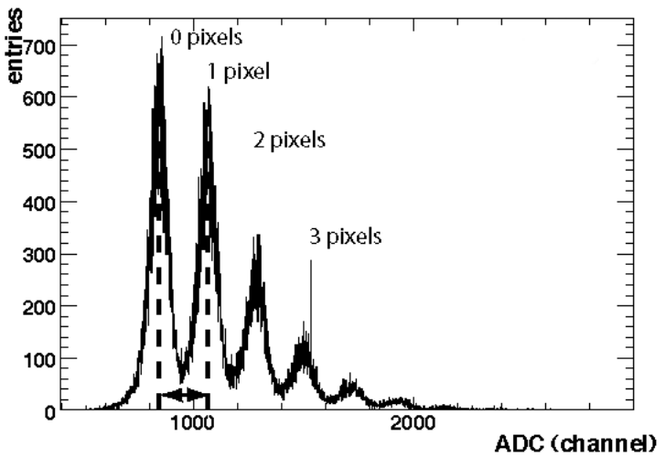

Fig. 10. SiPM response to low intensity light. The first peak corresponds to the pedestal, other peaks are signals from one, two and three photoelectrons. The peaks are equidistant, the distance indicated by ↔ is proportional to SiPM gain. The scale is in ADC counts corresponding to the charge of the SiPM signal (1 ADC count is 0.25 pC).

Also the stability of the SiPM response curve in the whole dynamic range must be known for offline corrections. These tasks are achieved with the calibration and monitoring system.

The photodetector gain and its saturation are monitored by UV LED flashes (λ = 400 nm) which are delivered to each tile via clear fibres. For the response curve measurement, the LED pulses must be tuneable in intensity from a few photoelectrons to thousands photoelectrons on the SiPM. The upper range value is given by the maximal expected rate of particles in a calorimeter cell which was obtained from shower simulations and is about 100 particles (MIPs). For the gain setting of about 13 photoelectrons/MIP, we arrive at the highest signals of ~ 1300 photoelectrons.

The LED light pulse is ~ 10 ns wide and of trapezoidal shape. Particle ionization in the scintillator tile produces typically one order of magnitude shorter light pulses. The LED light pulse intensity is proportional to the pulse length. To get intensity on the level of a thousand of photoelectrons it is easier to use longer pulses. The pulse length is limited by the after-pulsing property of the photodetector and by choosing the value of the quenching resistor, the afterpulsing can be almost avoided. The low intensity light is used for gain calibration and uses the unique sensitivity of SiPM to single photoelectrons (see Fig. 10).

The scheme of the electronic circuit for LED light pulses – LED driver – is displayed in Fig. 11. The design is particularly optimized for the generation of nearly rectangular fast pulses (rise and fall time ~1 ns) with variable amplitude in a large dynamical range. For these reasons we abandoned the classical approach of discharging a capacitor to the LED (Apuhn et. al., 1997). We adopted a scheme using the IXLD02 integrated circuit developed for semiconductor lasers. Based on the Tcalib signal from the calorimeter control, three signals are derived. The ENable, DRVpulse, and invDRVpulse control the output stage of LED driver. The ENable pulse wakes up the circuit. The LED is reversely polarized until the arrival of the DRVpulse which switches on the transistor Q1 for about 10 ns and the LED makes a flash. The role of the invDRVpulse is to improve the rise and fall time of the LED flash by switching complementary the transistor Q2 and since that, LED is quickly reversed till the end of ENable. The intensity of the LED light amplitude is controlled by the Vcalib amplitude in the control current sink CCS. The LED light emission characteristics do not change with the increase of the LED current in the range 10 µA to 10 mA (Polak, 2006).

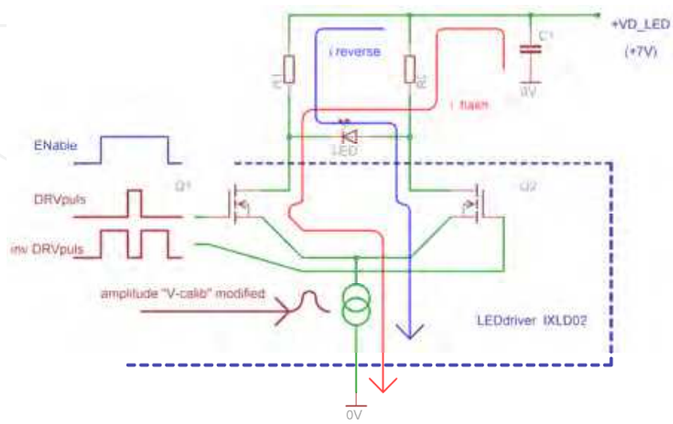

Fig. 11. The principle scheme of the LED driver. IXLD02 is the IC which produces rectangular pulses based on signals Ebable and DRV. The invDRVpulse improves the pulse shape. The pulse amplitude is controlled by the Vcalib value.

In order to reduce light fluctuations among LEDs, LEDs were sorted into groups with a similar light-intensity profile. One LED supplied 18 tiles and a monitoring PIN diode. Since PIN photodiodes have a gain of unity, an additional charge-sensitive preamplifier for the PIN photodiode readout was envisaged. The presence of a high-gain preamplifier directly on the board in the vicinity of the power signals for LEDs, however, has turned out to be a source of cross talk. One calorimeter plane of 216 tiles required 12 LEDs and 12 PIN diodes. The electronics providing LED pulses is laid on the Calibration and Monitoring Board (CMB) and located along one side of the calorimeter plane opposite to the read-out electronics and bias voltage supply. Another task of the CMB consists of reading out the temperature sensors via a 12 bit ADC. The temperature values are sent to the slow control system via a CANbus interface. One CMB operates seven temperature sensors, two sensors directly located on the readout board and five sensors distributed across the centre of the cassette. The sensors consisting of integrated circuits of type LM35DM produced by National Semiconductor are placed in a 1.5 mm high SMD socket. Their absolute accuracy is < 0.6°C. A microprocessor PIC 18F448 in association with a CAN controller interface (PCA82C250) provides the communication of the CMB with the slow control system. We have not observed any noise pickup in the CMB.

8. Saturation correction

As already mentioned in section 3, this photodetector is highly non-linear device due to finite number of pixels, the finite recovery time given by the value of internal resistor R_{pixel} and also due to the crosstalk. The number of fired pixels N_{pix} in the simplest case can be approximated by the formula $N_{pix} = N_{avail} (1 - \exp (-\varepsilon N_{ph} / N_{avail}))$ for number of photons N_{ph} impinging uniformly and simultaneously on the total number of available pixels N_{avail} of the photocathode, ε is the photon detection efficiency (defined in section 3). This simplest form has been used for the MPPCs of the ScECAL (Kotera, 2010). The number of pixels obtained from the fit to the measured response curve was $N_{avail} = 2424$ for photodetector with 1600 pixels. The large value of N_{avail} from the fit was attributed to the short recovery time of some pixels. The pixel then can fire for a second time on late photons radiated from the WLS fibre. In ref. (Adloff et al., 2011) where properties of SiPMs in the AHCAL are described, the sum of two exponentials was used which takes into account possible non homogeneity in the light transmission between the WLS fibre and the photodetector photocathode. The formula can in principle be extended to the sum of more exponentials to take into account other possible non-homogeneities. The response function for each SiPM was inverted and the correction function for one SiPM is shown in Fig. 12. The response of all SiPMs of the AHCAL clearly showed that on average only 80% of the photodetector pixels are used. This was explained by the different geometry cross-section of the WLS fibre with 1 mm diameter that covers effectively 78.5% of the square surface of the photocathode 1x1 mm^2.

The detailed study of the parameter N_{avail} was thereafter done for all SiPMs using only the response at the highest LED light intensities using the single exponential $N_{pix} = N_{avail} [1-\exp(-(X-C)*B)]$, X is the voltage on the LED. The constant C takes into account the LED starts to emit at voltage $X = C$. Fits to data allowed a value of N_{avail} to be obtained for 83% of SiPMs with a spread of 0.7% around the value 1156 pixels * 0.8 = 928 pixels (Zalesak, 2011). For the remaining SiPMs the nominal value of $N_{avail} = 928$ pixels can be used.

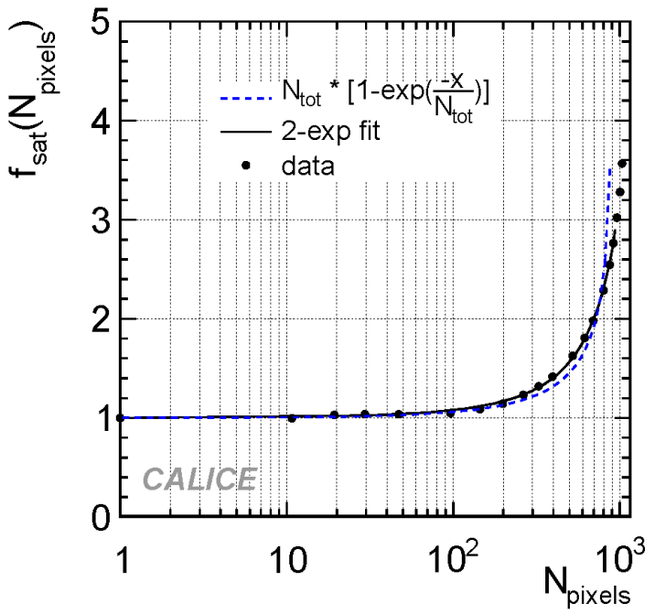

Fig. 12. The SiPM non-linearity correction function. The points are values for one SiPM. The solid line is double exponential fit, the dashed line is the single exponential fit, $N_{tot} = N_{avail}$ used in the text.

9. New developments

The experience with the physics prototypes will be used in the design of calorimeters for the full size detector at the LC. E.g. the hadron calorimeter will occupy volume of ~ 80 m^3 and with scintillator tiles 30 mm x 30 mm it will have ~ 3.2 10^6 channels (Abe et al., 2010). The readout electronics will be integrated in the calorimeter volume to minimize the dead space. The electronics has to have low power consumption to minimize the demands on cooling. The detector parts must be designed to allow the industrial production. As the next step technological prototypes are being designed and built and will meet most of these requirements.

9.1 Hadron calorimeter

The design of a half-octant of AHCAL is shown in Fig. 13. A single detection layer, one of 48 making the full depth of the calorimeter, consists typically of 16 HCAL Base Units (HBU). The HBU (Fig. 14) is the smallest component of the calorimeter with 144 scintillator tiles. To minimize the depth of the calorimeter, the tile thickness was decreased from 5 to 3 mm. Each tile will be equipped with a new type of SiPM (Sefkow, 2006).

The WLS fibre will be placed in a straight groove in the tile to avoid the time-consuming process of fibre bending (see Fig. 15). The thinner scintillator tile affects the SiPM design. We plan to use CPTA MRS APDs with the number of pixels reduced to ≤ 800 (Buanes et al., 2010). These SiPMs have smaller cross-talk and noise and lower sensitivity to temperature and voltage variations than SiPMs from PULSAR used in the AHCAL physics prototype. The latest tests in the positron beam showed a very good functionality with a signal of ~ 15 pixels/MIP.

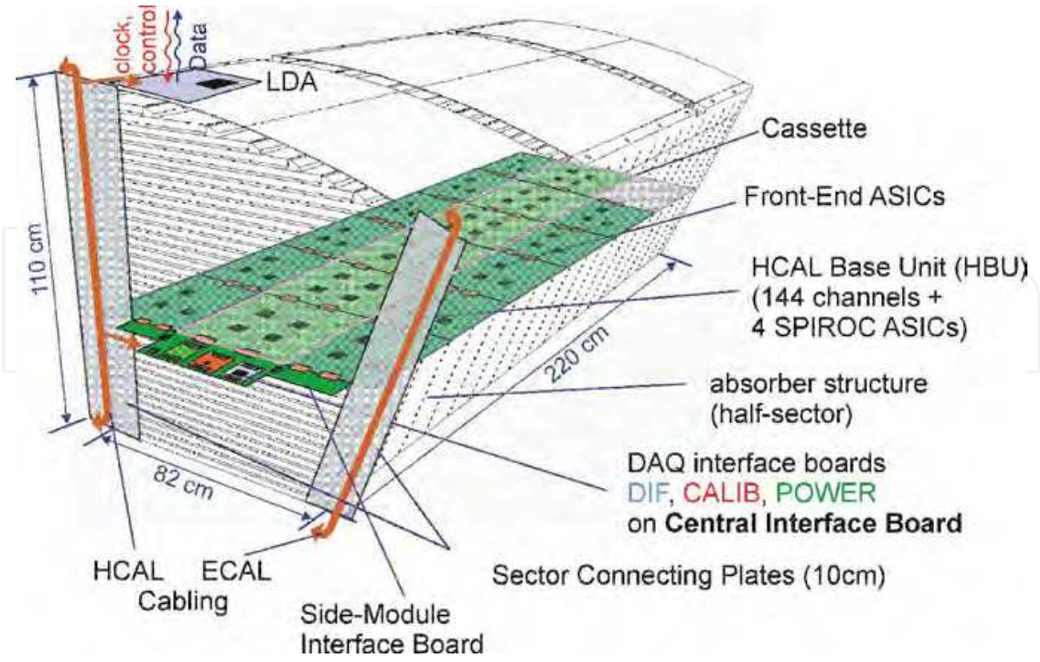

Fig. 13. View of the 1/16 of the AHCAL barrel wheel. One of 48 detection layers is shown in colour. It is made of HCAL base units HBUs. The service modules DAQ, DIF, CALIB and POWER are outside the detector volume.

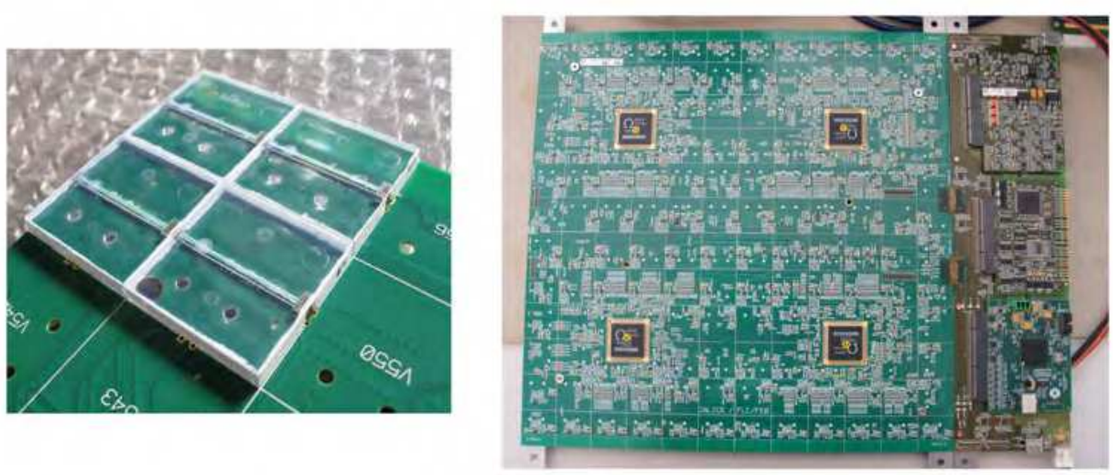

Fig. 14. (left) Four scintillation tiles assembled on the bottom of the HBU. The top side of the HBU. (right) has the front-end electronics with 4 ASICs and calibration LEDs for 144 tiles. The HBU is connected from right to DIF (bottom), CALIB (middle) and POWER (top) boards.

The new front-end ASIC chip powers, reads and amplifies the signal from 36 photodetectors (twice more than in the physics prototype). A 12-bit ADC in the chip digitizes the photodetector amplitude and provides fully digitized output. The size of the chip is reduced to 30 mm² using the 0.35 μm technology. The chip can be operated in the power pulsing mode with significantly reduced power consumption 25 μW (40 μW) per channel (including

SiPM bias voltage). After packaging the ASIC size is 28x28x1.4 mm^3 (Raux, 2008). The first experience with the ASIC performance was recently reported (Terwort, 2011).

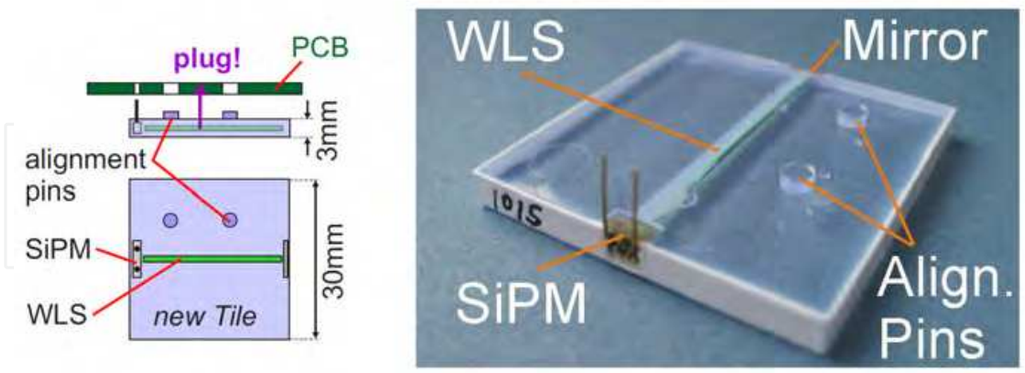

Fig. 15. The construction drawing (left) and the photo (right) of the scintillator tile with straight WLS fibre and SiPM attached to its end. The alignment pins in the tile fix the tile into the PCB.

The response of SiPMs is controlled by new calibration and monitoring system. Two concepts are currently under development:

- Each channel incorporates a SMD LED embedded on the HBU. LED illuminates the scintillator through a hole in the PCB. The control of LEDs is provided by the CALIB module on side of the HBU. This system is already implemented in the setup of Fig. 14. Each LED has its own driver – a low-component-count and effective circuit that discharges a capacitor through the LED. It was observed that pulse length depends on the LED type – blue LED generates long pulses ~40 ns and UV LEDs fast pulses ~8 ns long. This behaviour was explained by the different internal structure of LEDs which leads to different internal LED capacitance. At low intensity the driver generates single photon electron spectra for gain calibration purposes. The driver was finally tuned to deliver also high intensity light up to saturation mode of the SiPM with 796 pixels (Sauer et al., 2011).
- A luminous space LED with its driver placed on a special board. The light is distributed via notched fibres to rows of tiles (up to 72 tiles/fibre with the light output homogeneity of 20%). The fibre is positioned on the HBU on the top side. The notch flashes light through a hole in the PCB to the scintillator. The LED driver works as a heavily dumped quasi-resonant sine waves generator, where the first positive half-wave generates light and negative half-wave bias the LED negatively. Following sine waves are small and keep the LED reverse biased (non-shining mode) (Kvasnicka, 2011). It utilizes a toroidal inductor embedded in the PCB, and produces almost sinusoidal pulses which reduce the electromagnetic interference. For the toroid inductance 35 nH, the LED flash has fixed length of 3.5 ns. The LED amplitude is tuneable from low intensity light for the SiPM gain calibration to the high intensity signal equivalent to 200 MIPs in the tile. For the driver circuit scheme and the PCB with the circuit and toroidal inductor see Fig. 16.

As can be seen in Fig. 13 and in a greater detail in Fig. 14 (right), each detection plane is interfaced with the Data AcQuisition (DAQ) system via Detector InterFace (DIF) board. The calibration system is steered by the CALIB board and the power module (POWER)

distributes necessary voltages and arranges the power pulsing regime. All modules are available and are currently under test to commission the communication between different systems. The detection plane or its part will undergo beam tests in the year 2012.

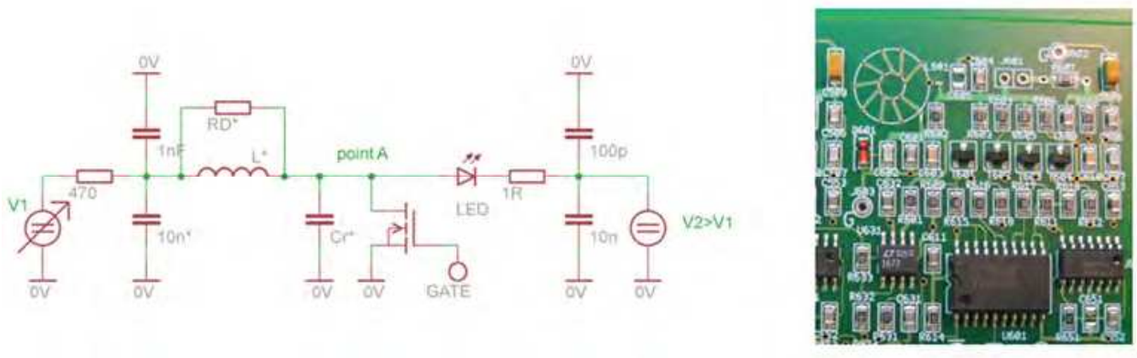

Fig. 16. (left) Driver circuit scheme. (right) LED driver on PCB with toroidal inductor at the top left.

9.2 Scintillator ECAL

The development of the next generation of the scintillator electromagnetic calorimeter will be done together with the SiW ECAL (Takeshita, 2011). To decrease the price of the calorimeter determined mainly by the price of the silicon sensors, it was decided to replace approximately half of the silicon sensor planes in the ECAL by scintillator planes with orthogonal strips. As the size of the silicon sensors was decreased from 10 mm x 10 mm to 5 mm x 5 mm, the width of scintillator strips will be correspondingly reduced from 10 mm to 5 mm. The scintillator thickness will decrease from 5 mm to 2 mm to better match the width of silicon layers. It is no longer possible to insert a WLS fibre inside such a thin scintillator. Therefore a new R&D program is envisaged aimed at the direct coupling of the MPPC to the tile side. This will further simplify production of large detector.

10. Conclusion

Prototypes of electromagnetic and hadron calorimeters with scintillator and embedded photodetectors for a detector at a future linear collider have been successfully built. The calorimeters with unprecedented granularity were successfully tested in electron, muon and hadron beams at accelerators in CERN and Fermilab. Commissioning and operation in the test beam demonstrated that calorimeters perform according to expectations. Test data were used to set up and tune the energy calibration of calorimeters. In case of the AHCAL, two new software correction methods were developed which compensate for the calorimeter's higher response to electrons. The application of both methods to the test beam data results in improvement in the energy resolution of the hadron calorimeter by 21% in the energy range 10–80 GeV.

New semiconductor photodetectors were developed for both calorimeters which provide gain of a classical photomultiplier but in a photodetector with millimetre dimensions and bias voltage of ~ 60 V. The new photodetector is embedded directly in the scintillator tile/bar and significantly reduces the calorimeter dead space and simplifies calorimeter construction. More than 10000 of these photodetectors in total were produced by

MEPHi/PULSAR (called silicon photomultipliers) and Hamamatsu Photonic (called pixelated photon counters). The successful operation of these detectors over a period of several years opened the door for their use in applications in material research and medicine.

The experience with the physics prototypes of calorimeters will be used in the design of calorimeters for the full size detector at the linear collider. Here the total number of channels will be of the order of millions. This brings new challenges especially on electronics which must be integrated in the calorimeter volume to minimize the dead space. The electronics must have low power consumption to minimize demands on cooling. The first versions of read-out ASICs were developed. The ASIC integrates functions performed previously by the data acquisition electronics. The next generation of calorimeter prototypes has started to be built and will be ready for beam tests in 2012.

11. Acknowledgment

I would like to thank to all my colleagues from the CALICE collaboration for the excellent work done during the construction of calorimeters, their operation and convincing results from the beam tests. Especially I want to thank to M. Danilov, G. Eigen, E. Garutti, K. Kotera, J. Kvasnička, V. Morgunov, I. Polák, F. Sefkow, D. Ward and J. Zálešák for discussions, comments, and providing me with the material for this contribution.

This work was supported by the Ministry of Education, Youth and Sports of the Czech Republic under the projects AV0 Z3407391, AV0 Z10100502, LC527 and LA09042.

12. References

Abe, T., et al. (2010). The International Large Detector: Letter of Intent, In: *FERMILAB-LOI-2010-03, FERMILAB-PUB-09-682-E, DESY-2009-87, KEK-REPORT-2009-6*, ISBN 978-3-935702-42-3

Adloff, C., et. al. (CALICE Collaboration). (2010a). Construction and commissioning of the CALICE analog calorimeter prototype. *Journal of Instrumentation*, Vol.2010, No. 5, (May 2010), p. P05004, ISSN 1748-0221, e-Print: arXiv:1003.2662 [physics.ins-det]

Adloff, C., et al. (CALICE Collaboration). (2010b). Study of the interactions of pions in the CALICE silicon-tungsten calorimeter prototype. *Journal of Instrumentation*, Vol.2010, No. 5, (May 2010), pp. P05007, ISSN 1748-0221, e-Print: arXiv:1004.4996 [physics.ins-det]

Adloff, C., et. al. (CALICE Collaboration). (2011). Electromagnetic response of a highly granular hadronic calorimeter. *Journal of Instrumentation*, Vol.2011, No. 6, (June 2011), p. P04003, ISSN 1748-0221, e-Print: arXiv:1012.4343 [physics.ins-det]

Apuhn R.-D., et. al. (1997). The H1 lead / scintillating fiber calorimeter, *Nuclear Instruments & Methods in Physics Research*, Vol.A386, (1997), pp.397-408, ISSN 0168-9002

Bilki, B., et al. (2009). Measurement of Positron Showers with a Digital Hadron Calorimeter. *Journal of Instrumentation*, Vol.2009, No.4, (April 2009), p. P04006, ISSN 1748-0221, e-Print: arXiv: 0902.1699 [physics.ins-det]

Bondarenko, G., Buzhan, P., Dolgoshein, B., Golovin, V., Gushin, E., Ilyin, A., Kaplin, V., Karakash, A., Klanner, R., Pokachalov, V., Popova, E. & Smirnov, S. (2000). Limited Geiger-mode microcell silicon photodiode: New results. *Nuclear Instruments & Methods in Physics Research*, Vol.A422, No.1-3, (March 2000), pp. 187-192, ISSN 0168-9002

Brient, J.-C. & Videau, H. (2001). Calorimetry at the future e+e- collider, *Proceedings of APS/DFB/DBP summer study on the future of particle physics,* Snowmass, Colorado, USA, June30-July21, 2001

Buanes, T., Danilov, M., Eigen, G., Göttlicher, P., Markin, O., Reinecke, M. & Tarkovski, E. (2010. The CALICE hadron scintillator tile calorimeter prototype, *Nuclear Instruments & Methods in Physics Research*, Vol.A623, No.1, (November 2010), pp. 342-4, ISSN 0168-9002

Buzhan, P., Dolgoshein, B., Ilyin, A., Kantserov V., Kaplin, V., Karakash, A., Pleshko, A., Popova, E., Smirnov, S., Volkov, Yu., Filatov, L., Klemin, S. & Kayumov, F. (2001). An advanced study of silicon photomultiplier. *ICFA Instrumentation Bulletin*, Vol.Fall2001, No.3, (2001), pp. 1-14, Available from: http://www.slac.stanford.edu/pubs/icfa/fall01/paper3/paper3b.html

Calice. (n.d.). CALICE Collaboration, Available from: https://twiki.cern.ch/twiki/bin/view/CALICE/CaliceCollaboration

Chadeeva, M. (2011). Software Compensation using the CALICE calorimeters, *Proceedings of the LCWS 2011*, Granada, Spain, September 26-30, 2011

Chakraborty, D. (2005). The Tail-Catcher/Muon Tracker for the CALICE Test Beam, *Proceedings of the 2005 International Linear Collider Workshop*, PSN 0919, Stanford, California, U.S.A, March 18 – 22, 2005. Available from: http://www.slac.stanford.edu/econf/C050318/proceedings.htm

CLIC. (2011). The Compact Linear Collider Study, Available from: http://clic-study.org

Cvach, J. (2002). Calorimetry at a future e^+e^- collider, *Proceedings of the 31th international conference on high energy physics (ICHEP)*, pp. 922-926, ISBN 0-444-51343-4, Amsterdam, The Netherlands, July 23-29, 2002

Danilov, M. (2007a). Comparison of different multipixel Geiger photodiodes and tile-photodetector couplings, *Proceedings of the Linear Collider Workshop LCWS 2007 and ILC 2007*, pp. , ISBN 978-3-935702-27-0, Hamburg, Germany, May 30 – June 3, 2007. Available from: http://lcws07.desy.de/e14/index_eng.html

Danilov, M. (2007b). Scintillator tile hadron calorimeter with novel SiPM readout. *Nuclear Instruments & Methods in Physics Research*, Vol.A581, No.1-2, (October 2007), pp. 451-456, ISSN 0168-9002

Eigen, G. (2006). The CALICE scintillator HCAL test beam prototype, *Proceedings of the 12th International Conference on Calorimetry in High Energy Physics, AIP Conference Proceedings Series, High Energy Physics Subseries*, Vol. 867., 2006, XXIV, ISBN: 978-0-7354-0364-2, Chicago, Illinois, U.S.A., June 5-9, 2006

ILC. (2007). ILC Reference Design Report, August 2007, Available from: http://www.linearcollider.org/about/Publivations/Reference-Design_Report

Kotera, K. (2010). Study of the Granular Electromagnetic Calorimeter with PPDs and Scintillator Strips, *Proceedings of the 12th Vienna Conference on Instrumentation VCI2010*, Vienna, Austria, February 15 – 20, 2010. Available from http://indico.cern.ch/getFile.py/access?contribId=182&resId=0&materialId=paper&confId=51276

Kvasnicka, J. (2011). LED calibration systems for CALICE hadron calorimeter, *Proceedings of the 2nd conference on Technology and Instrumentation in Particle Physics TIPP 2011*, Chicago, Illinois, U.S.A., June 8-14, 2011

Laktineh, I. (2011). Construction of a technological semi-digital hadronic calorimeter using GRPC. *Journal of Physics: Conference Series*, Vol.293 (2011) p. 012077, ISSN 1742-6596

Morgunov, V.L. (2002). Calorimetry design with energy-flow concept, *Proceedings of the 10th conference on calorimetry (Calor02)*, pp. 70-84, ISBN 981-238-157-0, Pasadena, California, USA, March 25-29, 2002

Musienko, Yu. (2011). State of the art in SiPM's. *The Technology Transfer Network for Particle, Astroparticle and nuclear physics event*, CERN, Geneva, Switzerland, February 16 – 17, 2011. Available from: http://indico.cern.ch/getFile.py/access?contribId=11&sessionId=7&resId=0&materialId=slides&confId=117424

Polak, I. (2006). Development of Calibration system for AHCAL, *International Linear Collider (ILC) Workshop*, Valencia, Spain, November 6-10, 2006. Available from: http://www-hep2.fzu.cz/calice/files/ECFA_Valencia.Ivo_CMB_Devel_nov06.pdf]

Raux L. (2008). SPIROC Measurement: Silicon Photomultiplier Integrated Readout Chip for ILC, *Proceedings of the 2008 IEEE Nuclear Science Symposium (NSS08)*, Dresden Germany, 2008

Repond, J., et al. (CALICE Collaboration). (2008). Design and Electronics Commissioning of the Physics Prototype of a Si-W Electromagnetic Calorimeter for the International Linear Collider. *Journal of Instrumentation*, Vol.2008, No. 3, (March 2008), pp. P08001, ISSN 1748-0221, e-Print: arXiv:0805.4833 [physics.ins-det]

Sauer, J., Götze, M., Weber, S. & Zeitnitz, C. (2011). Concept and status of the LED calibration system, *CALICE Collaboration meeting*, CERN Geneva, Switzerland, May 19-21, 2011. Available from: http://indico.cern.ch/contributionDisplay.py?sessionId=10&contribId=7&confId=136864

Sakuma, T. (2010). *Performance Study of Prototype Fine-granular EM Calorimeter for ILC*. Shinshu University, Shinshu, Japan, Master thesis, 01.02.2010. Available from: http://hepl.shinshu-u.ac.jp/index.php?HE%20Lab%20Top%20Page%2FIntroduction%2FMaster%20Theses

Sefkow, F. (2006). MGPDs for calorimeter and muon systems: requirements and first experience in the CALICE test beam. *Proceedings of Science*, Vol.PD07 (2006), p. 003, ISSN 1824-8039

De La Taille, C., Martin-Chassard, G. & Raux, L. (2005). FLC−SIPM: Front-End Chip for SIPM Readout for ILC Analog HCAL, *Proceedings of the 2005 International Linear Collider Workshop*, PSN 0916, Stanford, California, U.S.A, March 18 – 22, 2005. Available from: http://www.slac.stanford.edu/econf/C050318/proceedings.htm

Thomson, M.A. (2009). Particle flow calorimetry and the PandoraPFA algorithm. *Nuclear Instruments & Methods in Physics Research*, Vol.A611, No.1, (November 2009), pp. 25-40, ISSN 0168-9002

Takeshita, T. (2011). ScECAL status report, *CALICE Collaboration meeting*, Heidelberg, Germany, September 14-16, 2011. Available from: http://ilcagenda.linearcollider.org/conferenceTimeTable.py?confId=5213#20110916

Terwort, M. (2011). Concept and status of the CALICE analog hadron calorimeter engineering prototype, *Proceedings of the 2nd conference on Technology and Instrumentation in Particle Physics TIPP 2011*, Chicago, Illinois, U.S.A., June 8-14, 2011

Zalesak, J. (2011). Calibration issues for the CALICE 1 m^3 AHCAL, *Proceedings of the LCWS 2011*, Granada, Spain, September 26-30, 2011

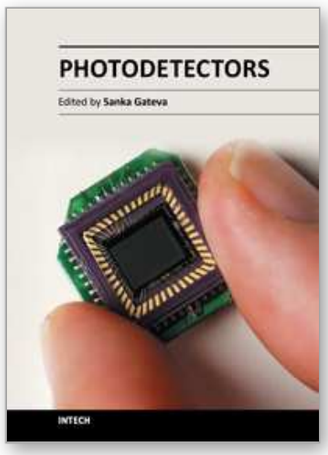

Photodetectors

Edited by Dr. Sanka Gateva

ISBN 978-953-51-0358-5
Hard cover, 460 pages
Publisher InTech
Published online 23, March, 2012
Published in print edition March, 2012

In this book some recent advances in development of photodetectors and photodetection systems for specific applications are included. In the first section of the book nine different types of photodetectors and their characteristics are presented. Next, some theoretical aspects and simulations are discussed. The last eight chapters are devoted to the development of photodetection systems for imaging, particle size analysis, transfers of time, measurement of vibrations, magnetic field, polarization of light, and particle energy. The book is addressed to students, engineers, and researchers working in the field of photonics and advanced technologies.

How to reference

In order to correctly reference this scholarly work, feel free to copy and paste the following:

Jaroslav Cvach and CALICE Collaboration (2012). Photodetectors in Calorimeters for the Linear Collider, Photodetectors, Dr. Sanka Gateva (Ed.), ISBN: 978-953-51-0358-5, InTech, Available from: http://www.intechopen.com/books/photodetectors/photodetectors-in-calorimeters-for-the-linear-collider

INTECH
open science | open minds

InTech Europe
University Campus STeP Ri
Slavka Krautzeka 83/A
51000 Rijeka, Croatia
Phone: +385 (51) 770 447
Fax: +385 (51) 686 166
www.intechopen.com

InTech China
Unit 405, Office Block, Hotel Equatorial Shanghai
No.65, Yan An Road (West), Shanghai, 200040, China
中国上海市延安西路65号上海国际贵都大饭店办公楼405单元
Phone: +86-21-62489820
Fax: +86-21-62489821

IntechOpen